Chapter 5

The Novel PAPR Reduction Schemes for O-OFDM-Based Visible Light Communications

Tian Zhang, Jun Yao and Shuxu Guo

Additional information is available at the end of the chapter

http://dx.doi.org/10.5772/intechopen.68763

Abstract

In this chapter, we propose two novel peak-to-average power ratio (PAPR) reduction schemes for the asymmetrically clipped optical orthogonal frequency division multiplexing (ACO-OFDM) scheme used in the visible light communications (VLC) system. In the first scheme, we implement the Toeplitz matrix based Gaussian blur method to reduce the high PAPR of ACO-OFDM at the transmitter and use the orthogonal matching pursuit algorithm to recover the original ACO-OFDM frame at the receiver. Simulation results show that for the 256-subcarrier ACO-OFDM system a ~6 dB improvement in PAPR is achieved compared with the original ACO-OFDM in terms of the complementary cumulative distribution function (CCDF), while maintaining a competitive bit-error rate performance compared with the ideal ACO-OFDM lower bound. In the second scheme, we propose an improved hybrid optical orthogonal frequency division multiplexing (O-OFDM) and pulse-width modulation (PWM) scheme to reduce the PAPR for ACO-OFDM. The bipolar O-OFDM signal without negative clipping is converted into a PWM format where the leading and trailing edges carry the frame synchronization and modulated information, respectively. The simulation and experimental results demonstrate that the proposed OFDM-PWM scheme offers a significant PAPR reduction compared to the ACO-OFDM with an improved bit error rate.

Keywords: visible light communications, peak-to-average power ratio, optical orthogonal frequency division multiplexing, Gaussian blur, pulse-width modulation

1. Introduction

The rapid development of solid state lighting technologies has made the visible light communications (VLCs) a promising complementary scheme in the widely used radio frequency

(RF)-based wireless communications in certain indoor and possible outdoor applications [1]. The main challenge of the VLC technology is the lack of sufficiently large bandwidth for modulation due to the fact that the white light emitting diodes (LEDs) used for VLC usually have a very small bandwidth, blue LED (BLED). Therefore, the transmission capacity of the VLC is limited [2]. In order to address this issue and make good use of the limited BLED with the aim of increasing the transmission throughput, a number of schemes including (i) blue filtering at the receiver (Rx) to remove the slow phosphor part of the spectrum, which increases BLED to ∼20 MHz but at the cost of high power loss, (ii) high spectrally efficient modulation schemes, such as a variant of optical orthogonal frequency division multiplexing (O-OFDM), discrete multi-tone modulation (DMT), and multi-band carrier-less amplitude and phase modulation, have been extensively investigated in the literature [3].

In intensity modulation and direct detection (IM/DD)-based VLC systems, the traditional complex and bipolar OFDM is modified to a real and unipolar format [4]. Though OFDM offers a number of advantages such as efficient use of the spectrum, there are many issues in OFDM-based VLC systems including (i) a high peak-to-average power ratio (PAPR), (ii) performance degradation due to non-linear power-current (P-I) characteristics of LEDs, (iii) limited support for dimming, and (iv) reduced throughput due to the use of longer cyclic prefix as a result of longer tails of the impulse response. Among these, the high PAPR is by far the most detrimental to the performance of OFDM-based VLC systems [5]. A higher PAPR would lead to more severe distortion and clipping because of the non-linear P-I characteristics of the LED [6]. This leads to a decreased signal-to-quantization noise ratio (SQNR) in both analog-to-digital (A/D) and digital-to-analog (D/A) converters while not fully utilizing the wide dynamic range of LEDs [7].

A number of techniques to mitigate the high PAPR requirement in O-OFDM have been reported in the literature including amplitude clipping [8], trellis coding, which reduces the average optical power [9], and block coding, which maps the vector of k-information bits to be transmitted and the vector of symbol amplitudes modulated onto the N-subcarrier [10] at the cost of increased transmission bandwidth. Signal transformation based on selected mapping (SLM) has also been used to reduce the signal peak values in O-OFDM systems [11]. In Ref. [12], the signal peak values are reduced by applying a pilot symbol (PS) phase rotation technique to the original OFDM signal. In Ref. [13], lower-order modulation on subcarriers, which suffers the most distortion, is used to achieve a high throughput for OFDM-VLC at a sampling rate of six times the available system bandwidth with reduced PAPR. The phase of PS is chosen based on the SLM algorithm while the maximum likelihood criterion is used at the Rx to estimate the PS. These techniques achieve PAPR reduction at the expense of increasing the transmit signal power, bit error rate (BER), data rate loss, computational complexity, and so on.

In this chapter, we introduce two novel PAPR reduction techniques for multicarrier transmission-based VLC system with some simulation and experiment demonstrations. The first scheme is named as Gaussian blur (GB) [14], which is enlightened by the blur operation used in image processing. The two-dimensional GB has been widely implemented in graphics software to reduce image noise and details by convolution operations [15]. Similar to this idea

of blurring images, we apply the one-dimensional GB to the time-domain signal of asymmetrically clipped optical orthogonal frequency division multiplexing (ACO-OFDM) system for reducing the high PAPR in VLC. Simulation results show that for the 256-subcarrier ACO-OFDM system, a ~6 dB improvement in PAPR is achieved in terms of the complementary cumulative distribution function (CCDF). However, the PAPR problem is only alleviated temporarily but not eliminated. In addition, considering that the indoor environment (i.e., the channel) is relatively static with no deep fading, the multipath-induced interference is not a major issue as is the case in an outdoor environment for RF-based wireless systems, and the use of O-OFDM needs additional operation to mitigate the high PAPR. Therefore, there is an open question: are there any advantages in transmitting the OFDM signal over a VLC channel or does it need to be converted into a digital format to avoid all the issues outlined above. To address this question, we further propose the second PAPR reduction scheme, which is named as the hybrid OFDM-PWM modulation [16], for converting the OFDM signal into a pulse-width modulation (PWM) format prior to IM of the LED in order to mitigate the high PAPR. The high PAPR in O-OFDM is no longer a major issue in OFDM-PWM as LEDs are only switched between "on" and "off". A similar technique is proposed in [17] where a linear mapping function is used to convert OFDM samples into PWM. However, the required bandwidth of proposed scheme in [17] exceeds the O-OFDM scheme, thus leading to a bit error rate (BER) penalty. In our improved OFDM-PWM scheme, we take advantage of the anti-symmetry property of the time-domain ACO-OFDM signal and hence convert only the first half of samples of the ACO-OFDM frame and extend the pulse width of PWM by a factor Nc. This ensures that the proposed OFDM-PWM has the same bandwidth requirement as the ACO-OFDM. Simulation and experimental results demonstrate that our proposed OPDM-PWM scheme has an improved BER performance compared with the original ACO-OFDM. Furthermore, the advantages of the scheme in Ref. [17], such as reduced PAPR, resilience to LED nonlinearity, and higher luminance level, are maintained.

2. The PAPR of O-OFDM and the CCDF of PAPR

OFDM is widely adopted in RF and optical communications including free space optics and VLC due to its huge data transmission capability, high spectral efficiency, and resilience to the channel-induced impairments. Although the OFDM modulated waveform has many advantages in both the RF and optical domain, its predominant drawback is that the signal profile has intermittent peaks that occur throughout the length of the OFDM signal contributing immensely to the peak-to-average power ratio (PAPR). With non-constant amplitude signals, it is important to improve the PAPR of those signals. The presence of these high peaks means that the optical source will have to operate outside its linear region to accommodate the full amplitude signal swings. This is very undesirable as it increases the level of distortion present in the transmitted signal, which results in poor system performance. Here, the definition of PAPR for a discrete ACO-OFDM signal $x(n)$ is given to evaluate the ratio of the maximum instantaneous power to the average power. To better approximate the PAPR of $x(n)$, the

O-OFDM signal samples $x(n)$ are obtained by oversampling L times. In [11], it is demonstrated that a fourfold oversampling factor ($L = 4$) is enough to provide an accurate measure of the PAPR value. Thus, the electrical PAPR of a single symbol O-OFDM signal is given as:

$$PAPR \triangleq \frac{\max|x(n)|^2}{E\left[|x(n)|^2\right]} \quad \text{for } 0 \le n \le N \times L-1 \tag{1}$$

where $E[.]$ denotes the statistical expectation, n is the number of samples for each OFDM frame in the time domain, and $x(n)$ is real and unipolar.

The cumulative distribution function (CDF) of the PAPR is one of the most frequently used performance measures for PAPR reduction techniques. In the literature, the complementary CDF (CCDF) is commonly used instead of the CDF itself. The CCDF of the PAPR denotes the probability that the PAPR of a data block exceeds a given threshold PAPR_0 as given by [18]:

$$\text{CCDF} = P(\text{PAPR} > \text{PAPR}_0) = 1-P(\text{PAPR} \le \text{PAPR}_0) = 1-\text{CDF} \tag{2}$$

3. GB-based PAPR reduction scheme

3.1. System overview

The block diagram of the GB-based ACO-OFDM system is depicted in **Figure 1**. In ACO-OFDM systems, the time-domain signal needs to be both real and unipolar. The bipolar signal at the output of Inverse Fast Fourier Transform (IFFT) is converted into unipolar by clipping the negative value to zero. Unlike the conventional ACO-OFDM system, in our scheme, the clipped output of IFFT is fed into theGaussian blur (GB) module to generate the alternative output sequence $S_i(n)$. Then, the sequence $S(n)$ with the lowest PAPR is applied to the optical driver module.

At the receiver side, the received signal is influenced by the noise sources in a real scenario. The dominant noise source in an indoor wireless optical channel is the ambient light-induced shot noise [19], which is modeled as the additive white Gaussian noise (AWGN). Thus, the received signal is given by:

$$y(n) = \eta \cdot \ S(n) \otimes h + Z(n), \ \ S(n) = \phi \cdot x(n) \tag{3}$$

where η is the photoelectric conversion efficiency, ϕ is a standard Toeplitz matrix, $\phi{\cdot}x(n)$ is the matrix representation of the Gaussian blur operation, $x(n)$ is the original ACO-OFDM signal, $S(n)$ is the alternative output signal with the lower PAPR, h is the channel response, $Z(n)$ is AWGN with zero mean and variance of δ_z^2, and $\otimes$ denotes the convolution operation.

We assume that the channel state information is perfectly known in advance. According to the transmitter design of ACO-OFDM, a half of the transmitted signals are clipped to be zeros. Therefore, the time-domain ACO-OFDM signal is a standard sparse signal adopted in the compressed sensing (CS) theory. Considering the special time-domain structure of ACO-OFDM symbols with the system complexity, we choose the orthogonal matching pursuit

http://dx.doi.org/10.5772/intechopen.68763

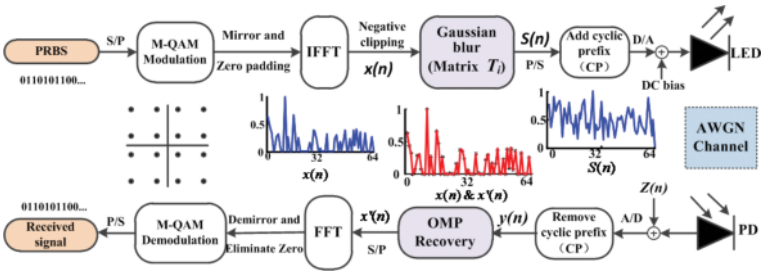

Figure 1. A block diagram of GB-based ACO-OFDM system is shown. S/P: serial-to-parallel converter, P/S: parallel-to-serial converter, and PD: photodetector.

(OMP) approach [20], which is widely used in sparse signal reconstruction in our simulation for recovering the original ACO-OFDM signal. Following the fast Fourier transformation (FFT) and demodulation process, we regenerate the original binary data stream.

3.2. GB algorithm

GB is a widely used image processing algorithm, which has the advantages of being very "smooth" and also circularly symmetric, so that edges and lines in various directions are treated similarly. It is well known that the two-dimensional GB operations are employed as the convolution in image processing to blur the images. The two-dimensional Gaussian kernel is defined as:

$$G(x,y) = \frac{1}{2\pi\delta^2} \cdot e^{\frac{-(x^2+y^2)}{2\delta^2}} \tag{4}$$

Applying GB to the original image $I(x, y)$ by convolving with Gaussian kernel function $G(x, y)$ to realize the blur operations, we have:

$$\begin{aligned} I_g(x,y) &= I(x,y) \otimes G(x,y) \\ &= \sum_{m,n} I(m,n) \cdot G(x-m, y-n) \end{aligned} \tag{5}$$

Similar to image processing, we apply the GB operation to the one-dimensional ACO-OFDM signal in optical communications. One-dimensional Gaussian kernel function $G(n)$ is implemented to convolve with the one-dimensional ACO-OFDM signal $x(n)$ as given by:

$$S(n) = \sum_{k=1}^{N} G(n-k)x(k), n = 1, 2 \ldots M \tag{6}$$

where N and M are the lengths of the ACO-OFDM signal and the alternative output $S(n)$, respectively.

Expanding Eq. (6), we have:

$$\begin{pmatrix} g(0) & g(-1) & \dots\ g(-N+1) \\ g(1) & g(0)\dots & g(-N+2) \\ \vdots & \vdots & \\ g(M-1) & g(M-2) & \dots g(M-N) \end{pmatrix} \cdot \begin{pmatrix} x_1 \\ x_2 \\ \vdots \\ x_N \end{pmatrix} = \begin{pmatrix} S_1 \\ S_2 \\ \vdots \\ S_M \end{pmatrix} \tag{7}$$

Corresponding to the CS theory, matrix $g(.)$ is the measurement matrix ϕ, matrix $x(.)$ is the sparse ACO-OFDM signal, and matrix $S(.)$ is the significant measurement, which has a lower PAPR compared with the original $x(.)$. From Eq. (7), we can see that the g(.) matrix is a standard Toeplitz matrix and its elements are Gaussian random variables with zero mean and variance of δ_z^2. Therefore, only $(M + N-1)$ elements are used to construct G, which means that only $\log_2(M + N-1)$ bits are needed to be transmitted as the side information [21]. In this module, a "blur" output sequence $S(n)$ is generated by taking the weighted sum of all the elements in $x(n)$ using the Gaussian distribution coefficients sequence $g(n)$ as the weights. Due to the random characteristic of the Gaussian function generated by the Matlab software which is used in our study, the generated output $S(n)$ is not the same as each other. Here, we construct a series of Toeplitz matrices T_i to obtain the lowest PAPR signal from $S_i(n)$, where i is the number of candidate matrices. Note that we only select the output signal $S_i(n)$ with the lowest PAPR for transmission.

Similar to the SLM method, the performance of the proposed scheme depends on the value of i and the elements of T. However, lower PAPR can be potentially attained for all ACO-OFDM signals as shown in **Table 1**.

To trade-off PAPR reduction and the system complexity, we have used $i = 6$ in our simulations to achieve ~6 dB improvement.

3.3. OMP recovery algorithm

The CS technique has been widely applied in signal reconstruction, medical imaging, radar, remote sensing, and other signal processing fields [22]. The main advantage of this theory is that it can recover original signals or images from far fewer samples or measurements. To realize this, CS has two fundamental criteria: (i) the original signal is sparse or compressible and (ii) the measurement matrix ϕ satisfies the restricted isometry property (RIP).

Suppose the transmission signal $x \in R^N$ is an N-dimensional sparse signal with sparsity K, $K \ll N$. The sparse reconstruction problem of CS is defined as recovering the sparse signal from the observed vector of measurements $S \in R^M$. The classical mathematical expression of CS measurement is given as:

$$S = \phi x + z \tag{8}$$

where $\phi \in R^{(M \times N)}$ is a known measurement matrix with $M \ll N$ and $z \in R^M$ denotes the measurement noise and model error. Note that measurement matrix ϕ needs to satisfy the RIP:

$$(1-\delta_k)\|x\|_{l_2}^2 \le \|\phi x\|_{l_2}^2 \le (1+\delta_k)\|x\|_{l_2}^2 \tag{9}$$

i_{th} PAPR	1	2	3	4	5	6	7	Original
x_1 (dB)	9.0	9.1	**8.0**	10.9	10.7	9.1	9.3	11.6
x_2 (dB)	9.3	9.5	8.4	8.4	9.0	**7.7**	11	12.4
x_3 (dB)	9.0	8.6	**7.5**	9.1	8.2	8.5	10.4	12.8

Note the simulation results obtained from three random 16-QAM ACO-OFDM signals (256-subcarrier). The numbers in bold are the minimum PAPR from a set of *i*- measurements.

Table 1. PAPR reduction results for original ACO-OFDM with GB.

where δ_k is a restricted isometric constant. For more details, please see [23]. Then, by resolving Eq. (8) with corresponding sparse signal reconstruction algorithm, one can obtain the estimation $\tilde{x}$. Two popular reconstruction algorithms are the convex optimization algorithm and the iterative greedy pursuit algorithm.

For the ACO-OFDM system, we can see that the asymmetrically clipped output of N-point IFFT is a sparse signal in the time domain, and the Toeplitz matrix composed of Gaussian random variables meets the restricted isometry property (RIP) standard as adopted in [23]. Therefore, the OMP algorithm, which has the advantages of lower computation complexity, rapid recovery speed, and higher reconstruction accuracy compared to other algorithms, can be employed in our scheme [24]. The equivalent electrical voltage signal $\tilde{Y}$ can be employed to reconstruct $\tilde{x}$ as outlined below:

$$\min\|\tilde{x}\|_1 \; s.t. \; T\tilde{x} = \tilde{Y} \tag{10}$$

where $T \in R^{(M\times N)}$ is the observation matrix ϕ and $\tilde{Y} \in R^M$ denotes the measured values of S. The OMP algorithm used in this chapter is summarized as below:

Step 1. Setting the residual value $r_0 = \tilde{Y}$, pre-recovery $\tilde{x} = 0$, and iterations number $n = 1.4{*}K$ ($n \geq K$), where K is the sparsity of x.

Step 2. Finding the max<T(:;col), r_0>and its position. Note that $M \geq C{*}K{*}\log_2(N/K)$, where C is a constant, depends on each instance.

Step 3. Calculating the reconstructed $\tilde{x}$ by min $\|\tilde{Y}-T\tilde{x}\|_2$ and updating the residual $r_n = \tilde{Y} - \frac{<T(\text{col}), \tilde{Y}>}{<T(\text{col}), T(\text{col})>} T(\text{col})$ by the least square algorithm.

Step 4. If the criterion has not been satisfied, then return to step 2.

3.4. Simulations and results

Simulations are conducted to compare the most widely used amplitude clipping method, classical SLM technique and the GB method, and the key parameters adopted are shown in **Table 2**.

Figure 2 shows the CCDF against the threshold PAPR_0 for the unmodified ACO-OFDM ($N = 256$) with the classical SLM, amplitude clipping (CL of 0.8), and the proposed method. Also shown is

Method	Subcarrier	Modulation	Parameter	Length
Clipping	256	16-QAM	CL = 0.8	—
SLM	256	16-QAM	$i = 6$	$N/4$
GB	256	16-QAM	$i = 6$	$M + N - 1$

Table 2. Simulation parameters for PAPR reduction schemes.

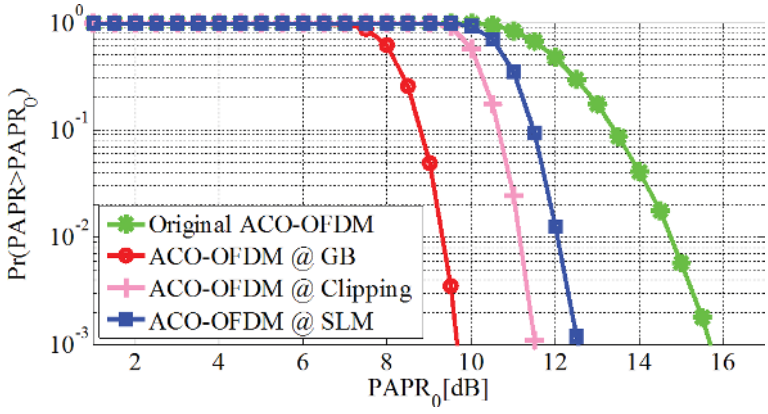

Figure 2. PAPR analysis for ACO-OFDM signals ($N = 256$) with SLM, clipping (CL = 0.8), and GB techniques ($i = 6$).

the plot for the original ACO-OFDM with no PAPR reduction scheme. The horizontal and vertical axes represent the threshold for the PAPR and the probability that the PAPR of a data block exceeds the threshold, respectively. It is shown that at CCDF of 10^{-3} the PAPR requirements are < 10, ~11.5, and > 12 dB for ACO-OFDMs with GB, amplitude clipping, and SLM, respectively, compared with the < 16 dB for the original ACO-OFDM. From the comparison, we can conclude that the proposed method offers improved PAPR reduction. Note that the simplest amplitude clipping method can achieve a much significant PAPR reduction at the cost of the unrecoverable performance degradation.

Next, we want to recover the original ACO-OFDM signal $x(n)$ from $\tilde{Y}$ at the receiver. For perfect reconstruction of the original signal, the row size of T must meet the following condition as outlined in [24]:

$$M \geq C \cdot K \cdot \log_2(N/K) \tag{11}$$

In ACO-OFDM, K is $N/2$. Therefore, M should be larger than the product of C and K to meet the signal reconstruction requirements. The signal reconstruction accuracy is evaluated by the reconstruct error (RE), which is given by:

$$\mathrm{RE} = \frac{\|x(n)' - x(n)\|_2}{\|x(n)\|_2} \tag{12}$$

where $x(n)^{'}$ is the reconstructed ACO-OFDM signal and $\|x(n)\|_2$ denotes the second moment norm, $\|x(n)\|_2 = \sqrt[2]{|x_1|^2 + |x_2|^2 + \cdots + |x_n|^2}, n = 1, 2, \ldots, N$.

Following a number of simulations with a range of C values shown in **Table 3**, we found that RE is reduced significantly with C increased from 1 to 2. However, for $C > 2$, the improvement in RE is very small, and $S(n)$ is longer than the original signal $x(n)$ measured in the time domain, since $M > N$. For the trade-off between RE and the data rate, we have selected $C = 2$ as the optimal value for the proposed system. Therefore, the Toeplitz matrix is a square matrix $T_{N\times N}$ with no incurred bandwidth penalty.

Figure 3 shows the reconstruction results for 256-subcarrier-based ACO-OFDM signal for an SNR of 30 dB using the OMP recovery algorithm. Note that in typical indoor VLC systems, the most widely used SNR is 30 dB [19]. We observe the faithful reconstruction of the distortion-less original signal for an SNR of 30 dB compared to the original ACO-OFDM signal. We have used $1 \times e^3$ random ACO-OFDM signals to calculate the RE over an SNR range of 2030 dB as shown in the inset in **Figure 3**. Note that the improvement in RE is < 0.06, which is far below the acceptable value of < 0.1 for the entire system performance.

Figure 4 illustrates the BER performance against the SNR for the uncoded 256-subcarrier ACO-OFDM with amplitude clipping and the proposed scheme. In practice, higher peak-to-average power ratio (PAPR) can lead to non-linear distortions and clipping in systems with peak-power limitations ($PAPR_0$), thus leading to degradation of the system BER performance. In this chapter, we define the ideal ACO-OFDM as having an infinite $PAPR_0$ and, therefore, the adverse effect of higher PAPR of the original ACO-OFDM signal is not considered in the BER

C	1.0	1.5	2.0	2.5	3.0	3.5	4.0
RE	14.25	0.43	0.031	0.022	0.021	0.020	0.017
Data rate	200%	133%	100%	80%	67%	57%	50%

Note that the simulation results are obtained for 256-subcarrier ACO-OFDM with an SNR of 30 dB.

Table 3. RE values and data rate against different C values.

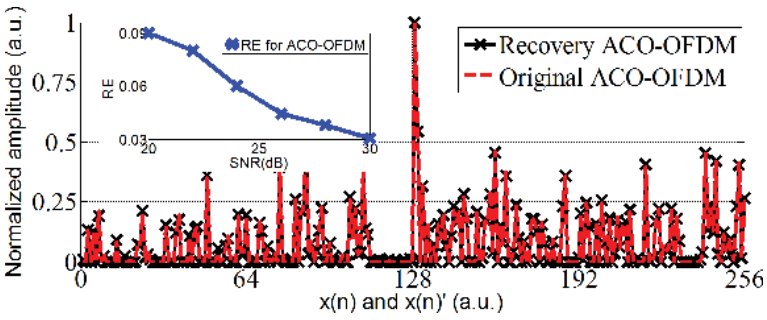

Figure 3. RE analysis for ACO-OFDM (with $N = 256$) for SNR of 30 dB. The inset shows the RE for 20 < SNR < 30 dB.

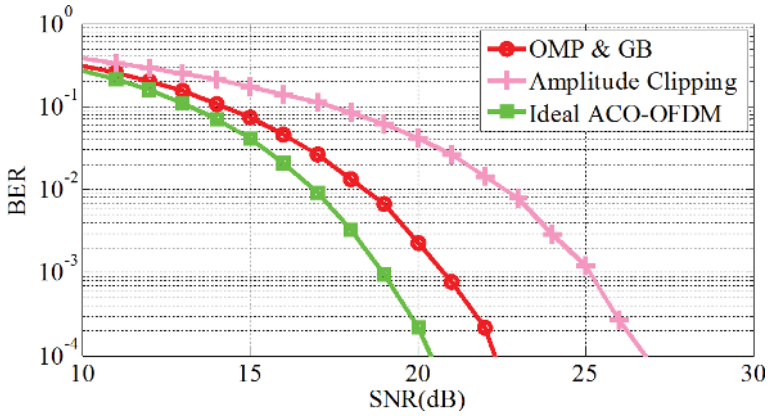

Figure 4. BER performance against the SNR for 256-subcarrier ACO-OFDM systems with amplitude clipping (CL = 0.8) and the proposed method ($i = 6$).

analysis. The BER performance of an ideal ACO-OFDM is used as a reference lower bound as in reference [25]. Thus, the recovery accuracy of the OMP algorithm is indirectly illustrated by the BER performance. At a BER of 10^{-4}, the proposed scheme requires only a ~2 dB of additional SNR compared to the ideal ACO-OFDM scheme. For ACO-OFDM with amplitude clipping, the SNR penalty is almost 5 dB compared to the proposed scheme. It also can be seen that when the SNR is larger than 20 dB, the BER of the proposed scheme is within the bound of the forward error correction (FEC) limits. And as for the VLC, these SNR values can be obtained by the need for illumination. From the results shown in **Figures 2–4**, we conclude that the proposed scheme can achieve a significant reduction in PAPR with a competitive recovery performance.

4. OFDM-PWM-based PAPR reduction scheme

4.1. System overview

The block diagram of the proposed OFDM-PWM scheme is shown in **Figure 5**, where the bipolar discrete-time O-OFDM samples $x(n)$ are first generated using the standard ACO-OFDM process as outlined in Ref. [26] but with no zero clipping operation prior to conversion to PWM. In the traditional O-OFDM such as DC-biased optical OFDM (DCO-OFDM), a DC bias is added to the signal before clipping the negative residual signals to ensure positive signal amplitude. However, due to a high PAPR, the DC bias required is very high, and it is also necessary to clip the DC-biased signal to clip the negative residue. ACO-OFDM overcomes the high DC-biased requirements by encoding information only on odd harmonics and clipping the negative signals at zero, which do not lead to any information loss [26]. Due to the Hermitian symmetry requirements to ensure a real-time-domain signal and with only odd subcarriers being used, only one-fourth of the subcarrier is actually encoded with the data. As a result, the spectral efficiency of ACO-OFDM is half of that of DCO-OFDM [27]. Therefore, the

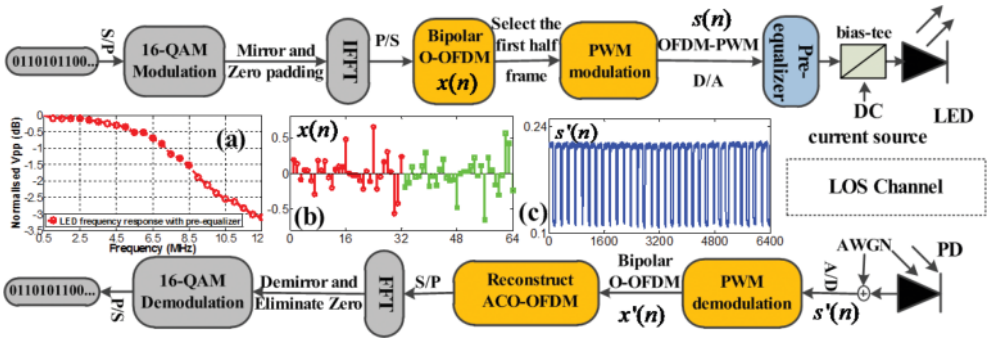

Figure 5. A block diagram of OFDM-PWM (a) LED frequency response with pre-equalizer, (b) bipolar O-OFDM before asymmetrical clipping, and (c) received OFDM-PWM waveform. LOS: line of sight.

resulting time-domain signal is a real-valued signal referred to as the O-OFDM frame with the anti-symmetry property as defined by Armstrong and Schmidt [27] and as shown in **Figure 5 (b)**:

$$x_k = -x_{k+N/2},\ 0 < k < N/2 \tag{13}$$

where N is the number of IFFT points.

In the OFDM-PWM scheme, since PWM can be used to linearly represent the bipolar signal, the zero clipping operation in ACO-OFDM is no longer necessary. Due to ACO-OFDM's anti-asymmetric time-domain characteristics, the first half of the bipolar samples (with no zero clipping) is sufficient to represent the entire unipolar ACO-OFDM. Hence, instead of converting the entire O-OFDM symbol into PWM, converting only the first $N/2$ samples would be sufficient, which does not lead to any loss of information. Thus, we discard the unnecessary last half of samples and save half of the time slots for further compensating the high bandwidth requirement for PWM, see **Figure 6(b)** (Digital OFDM-PWM). The generated OFDM-PWM signal is used for IM of the LED. At the receiver (Rx), the OFDM signal is extracted from OFDM-PWM, and the standard OFDM demodulation process is thereafter employed, which is the reverse of the transmitter (Tx) process, as outlined in Ref. [27].

PWM can be generated in the analog or digital domain. In the analogue PWM, the input signal (i.e., $x(n)$ in this case) is compared with a reference carrier signal (i.e., a ramp waveform) of frequency f_c as shown in **Figure 6(a)**. Note that the Nyquist condition $f_c \geq 2NT_s^{-1}$needs to be met, where T_s is the OFDM symbol period. In the digital PWM, the digital version of $x(n)$ is compared with a counter, which rests every 2^L where L is the bit resolution adopted in this chapter. In the PWM scheme, the falling edge carries the information whereas the rising edge is used for synchronization (more information on PWM can be found in Ref. [28]). Thus, the converted PWM signal shown in **Figure 6(a)** is given by:

$$PWM(t) = \begin{cases} C, & 0 \leq t \leq \tau \\ 0, & \tau < t \leq T_c \end{cases} \tag{14}$$

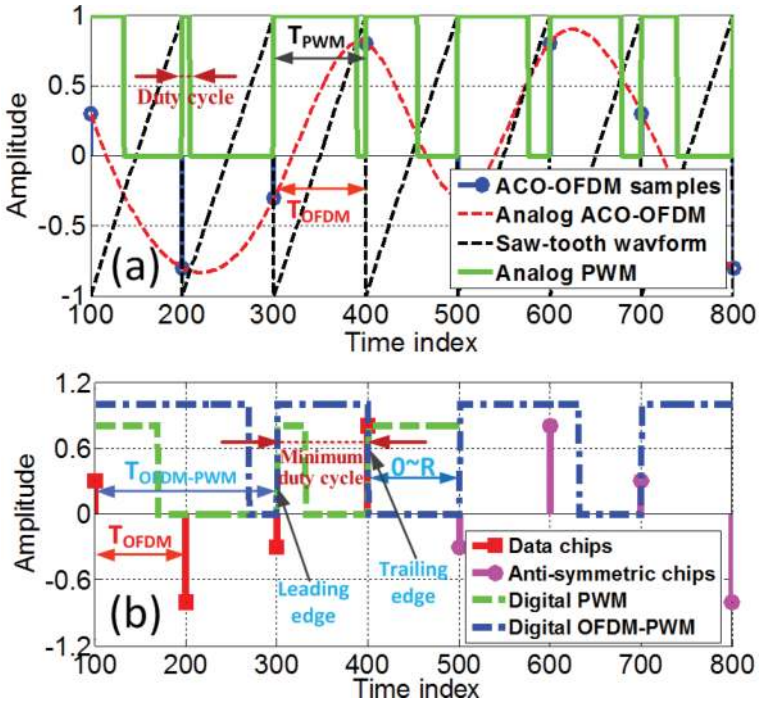

Figure 6. Time-domain waveforms for (a) ACO-OFDM, ramp, and PWM and (b) the process of the digital OFDM-PWM generation.

where T_c is the OFDM symbol sampling period, C is a constant corresponding to the peak amplitude of O-OFDM, and τ, given by Eq. (15), is the modulated pulse width that changes linearly with the instantaneous value of $x(n)$ as given by:

$$\tau(n) = \frac{x(n) - x_{\min}}{K} \tag{15}$$

where K is the PWM carrier signal slope factor or the modulation index defined as:

$$K = \frac{x_{\max} - x_{\min}}{T_c} \tag{16}$$

Note that $x_{\max}$ and $x_{\min}$ are the maximum and minimum amplitudes of O-OFDM symbols, respectively. In order to simplify generation of the digital PWM signal, the sampling period is divided into R discrete intervals with $R \geq M$, where M is quadrature amplitude modulation (QAM) modulation order. Therefore, Eqs. (15 and 16) are rewritten in a discrete form as:

$$K = \frac{x_{\max} - x_{\min}}{R} = \frac{(x(n) - x_{\min})}{N_\tau}, \quad n = 1, \ldots, N/2 \tag{17}$$

where N_τ is the corresponding discrete interval of $\tau(n)$.

In the converted PWM scheme, see **Figure 6(a)**, the minimum pulse duration $\tau(n)_{\min} = 1/R$ is significantly smaller than T_c. Hence, the bandwidth requirement for PWM is R times higher than ACO-OFDM. In order to overcome the high bandwidth requirement, the duty cycle of PWM signal is further extended by a factor of N_c, where $0 \le N_c \le R$ as shown in **Figure 6(b)** with blue lines. The value of N_c can be adjusted either to obtain a maximum throughput by setting $N_c = 0$ or a required dimming level by setting $N_c > 0$. In this study, we have increased the minimum pulse width to R by setting $N_c = R$ (see **Figure 6(b)**). This ensures that the PWM pulse duration is at least equal to or greater than T_c, which means that the proposed OFDM-PWM scheme has the same bandwidth requirement as that of ACO-OFDM. In addition, the increased time factor N_c is equal to the OFDM sample period, which indicates that we have taken full advantage of the last half time slots saved from the previous sampling part. Thus, the transformation from ACO-OFDM to OFDM-PWM is a lossless process. The proposed OFDM-PWM signal $s(n)$ is given by:

$$s(n) = \begin{cases} C, \ 0 \le N_{s(n)} \le (N_\tau + N_c) \\ 0, \ (N_\tau + N_c) < N_{s(n)} \le 2R \end{cases}, n = 1, \ldots, N/2 \tag{18}$$

where $N_s(n)$ is the total number of discrete intervals corresponding to the duty cycle of each OFDM-PWM signal.

Following the optical to electrical (O-E) conversion at the Rx, the received OFDM-PWM signal $s'(n)$ is given by:

$$s'(n) = \eta F[x(n)] \otimes h(n) + z(n) \tag{19}$$

where η is the photodiode responsibility, $F[.]$ is the transformation operation from O-OFDM to PWM, $x(n)$ is the bipolar O-OFDM signal, $h(n)$ is the channel impulse response, $z(n)$ is additive white Gaussian noise with zero mean and variance of δ_z^2, and $\otimes$ denotes the convolution operation. Note that here we have only considered the line of sight (LOS) propagation path in order to illustrate the concept.

As for the recovery of the original OFDM signal at the Rx, the sampling rate of OFDM-PWM must be at least $2R$ times of the ACO-OFDM signal to accurately detect the trailing edge of $s'(n)$. The total number of discrete intervals of $s'(n)$, that is $(N_t + N_c)$, is then estimated from the trailing edge position, and the first half of $x(n)$ is estimated using Eq. (17). Next, the standard ACO-OFDM demodulation process outlined in [3] is adopted to recover the transmitted signal.

4.2. Simulation results

Figure 7 shows the simulated PAPR for ACO-OFDM, ACO-OFDM with classical selected mapping (SLM) technique and the proposed OFDM-PWM method. Here, 16-QAM ACO-OFDM with 256-subcarrier is used as the baseline. The SLM method with six iterations is employed and compared with the proposed OFDM-PWM. **Figure 7** demonstrates that PAPR requirements at CCDF of 10^{-3} are ~3, >12, and < 16 dB for OFDM-PWM, ACO-OFDM with SLM, and ACO-OFDM, respectively. This clearly validates that the proposed OFDM-PWM offers significant PAPR reduction.

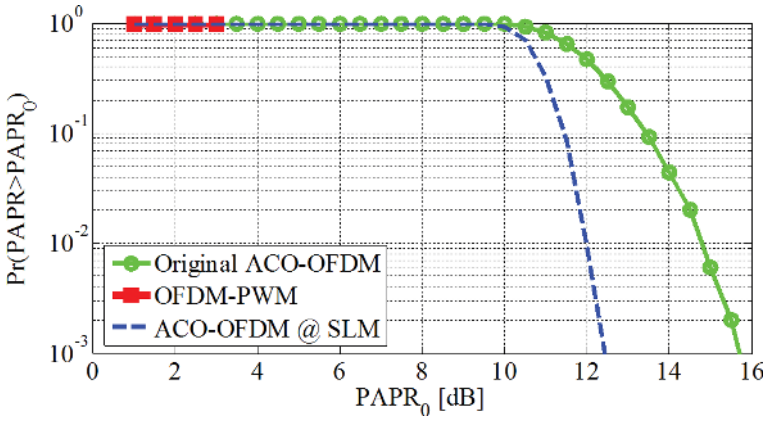

Figure 7. PAPR analysis for 16-QAM ACO-OFDM signals ($N = 256$) with SLM and OFDM-PWM.

Since the average duty cycle of OFDM-PWM is greater than Tc, the proposed OFDM-PWM scheme provides a higher illumination level provided that C is equal to the maximum amplitude of ACO-OFDM sample as shown in **Figure 8**.

Here, we calculate the average optical power of ACO-OFDM and OFDM-PWM to illustrate the illumination level. For the frame shown in **Figure 8**, the average power of OFDM-PWM is ∼4 times as much as the original ACO-OFDM frame. Therefore, C can be set to be smaller than the maximum amplitude of ACO-OFDM sample to achieve the desired illumination level and resilience to the $PAPR_0$ limit due to the non-linearity of the LED.

Next, we evaluate the BER performance of the proposed scheme for a line of sight (LOS) VLC link in Matlab environment. The key simulation parameters adopted in this work are summarized in **Table 4**.

Since the pulse-width variation in PWM is linearly proportional to the peak-to-peak amplitude, $v_{\text{p-p-OFDM,}}$ of the input signal (i.e., in this case, the O-OFDM), we need to know the time resolution corresponding to the amplitude resolution of the O-OFDM signal. We have selected a nominal value of R as given by:

$$R = \begin{cases} 100, & M \leq 16 \\ \alpha M, & M > 16 \end{cases} \tag{20}$$

where α is an empirical constant, which is set to be four in our simulation, and M is the QAM modulation order. For example, the values of R for 16- and 64-QAM are 100 and 256, respectively.

Figure 9 shows the simulated BER performance against the electrical SNR for OFDM-PWM and ACO-OFDM with 16- and 64-QAM. The simulation results clearly demonstrate that the OFDM-PWM outperforms ACO-OFDM. For example, at a BER of 10^{-4}, the SNR requirements are ∼14 and ∼18 dB for OFDM-PWM and ACO-OFDM, respectively, for 16-QAM, thus demonstrating an SNR gain of ∼4 dB using OFDM-PWM. The SNR gain is higher for the

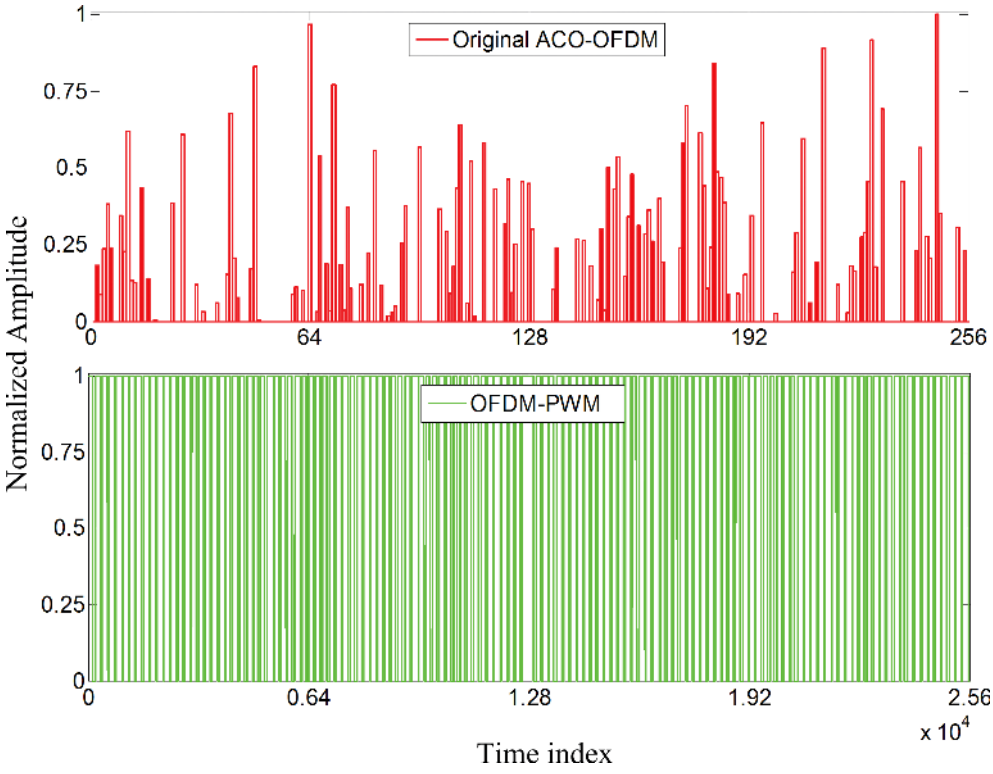

Figure 8. One frame of ACO-OFDM and OFDM-PWM with the same data information ($R = 100$ and 256-subcarriers).

Parameters	OFDM-PWM	ACO-OFDM
Modulation	16/64-QAM	16/64-QAM
No. of subcarriers	256	256
System bandwidth	10 MHz	10 MHZ
Date rate	40/60 Mbit/s	40/60 Mbit/s
Subdivisions	$R = 100/256$	–
Length of frame	25600/65536	256
Iteration	1000	1000

Table 4. Simulation parameters.

higher-order modulation with 64-QAM OFDM-PWM offering a gain of ∼9 dB compared to ACO-OFDM.

4.3. Experiment results

The experimental set-up shown in **Figure 10** has been developed to demonstrate the working principle of the proposed concept, validate the simulation results, and compare it with the

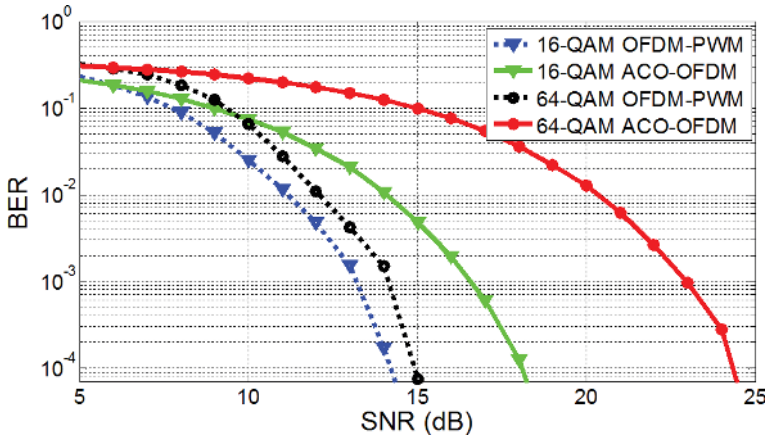

Figure 9. BER performance against the electrical SNR for OFDM-PWM and ACO-OFDM and with 16- and 64-QAM.

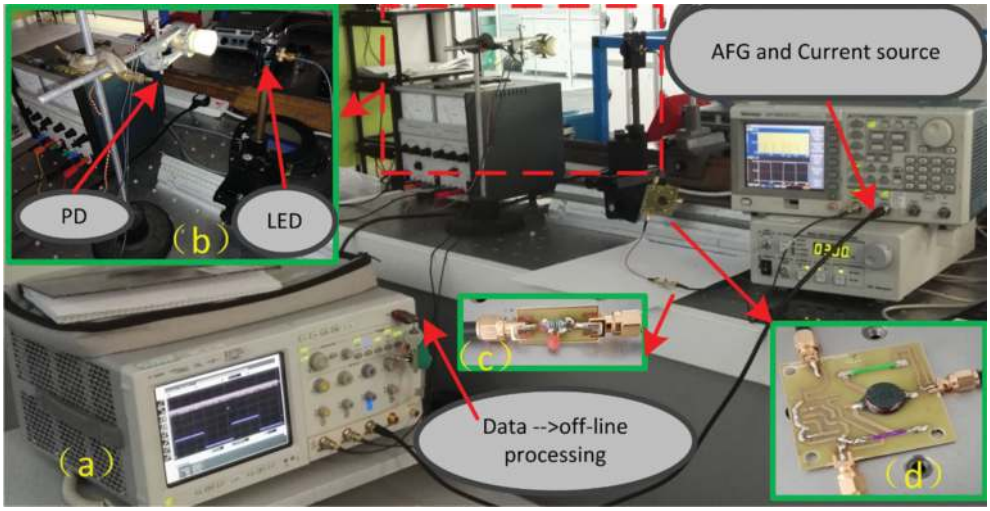

Figure 10. (a). The experimental setup for the proposed scheme. (b) The LED and PD, (c) the RC equalizer circuit, and (d) the DC-bias circuit.

standard ACO-OFDM under the same conditions. The frame frequency and frame sampling rate are shown in **Table 5**.

First, we generate the 16-QAM-based ACO-OFDM and OFDM-PWM signals using the algorithm outlined in Section 4.1. The waveforms are then loaded to the arbitrary function generator (Tektronix AFG 3022) using the LabVIEW 2014 interface. Following this, the output signal is pre-equalized using a simple resistance-capacitance (RC) network, see **Figure 10(c)**, and a DC-bias current I_{dc} of 200 mA is added prior to IM of the LED (Rebel Star 01). Note that

Parameters	OFDM-PWM	ACO-OFDM
Frame frequency f_{frame}	39 kHz	39 kHz
Frame sampling f_{sample}	5 G sample/s	50 M sample/s
DC-bias current	200 mA	200 mA
Modulation	16-QAM	16-QAM
No of random bits	256	256[1]

[1]Only one-fourth of the subcarrier is allocated for information bits in ACO-OFDM.

Table 5. Experimental parameters.

$I_{dc\text{-}ACO\text{-}OFDM} < I_{dc\text{-}DCO\text{-}OFDM}$, which is mainly used for illumination. Using an RC pre-equalizer network, BLED is increased from ~2 to 12 MHz [29] as shown in **Figure 5(a)**.

In practical VLC systems, LED non-linearity is important and should be considered, which limits the operating dynamic range, $PAPR_{0,}$ and consequently the SNR. Non-linearity arises due to the imperfection of the driving circuits and the number of emitted photons not being proportional to the injected current in the active region. The measured I-V curve for the LED used in this work is depicted in **Figure 11**, which shows linear and non-linear regions. A lower limit is like the turn-on voltage (TOV) and the saturation voltage.

The receiver's front end consists of an optical concentrator and a photodiode with differential amplifiers, the outputs of which are captured using a digital oscilloscope (Agilent Infinium 40GSa/s) for further offline processing. The oscilloscope sampling rates are set to 50 M and 5 G sample/s for ACO-OFDM and OFDM-PWM, respectively. Signals synchronization, down-sampling, and signal recovery are carried out offline. We then evaluate the BER performance of both ACO-OFDM and OFDM-PWM systems under the same conditions. For higher-order modulations (i.e., 64-QAM), the generated digital OFDM-PWM's length is 65, 536, which is beyond the 32 K memory of AFG 3022. Therefore, we could only transmit one frame of 16-QAM-based 256-subcarrier OFDM-PWM due to the limited memory of AFG3022. The received waveforms of ACO-OFDM and OFDM-PWM are shown in **Figure 12(a)** and **(b)**, respectively. The square waveforms shown are used to indicate the period of the OFDM signals. Following the offline processing, the original ACO-OFDM signal is fully recovered as shown in **Figure 12(c)**.

Figure 13 shows the estimated BER performance, which is obtained experimentally against the peak-to-peak amplitude, Vp-p values of 16-QAM-based ACO-OFDM and OFDM-PWM signals. Due to a limited number of transmitted bits, it is not feasible to accurately measure the BER below the FEC limit of 10^{-3}. Nonetheless, the graph clearly demonstrates the advantage of OFDM-PWM over ACO-OFDM, where it displays an improved BER performance in both linear and non-linear regions of the LED. For Vp-p < 2 V, the BER floor for OFDM-PWM is $<5 \times 10^{-3}$, whereas for ACO-OFDM, it is $> 10^{-1}$, except at Vp-p of 2, where the BER is 10^{-2}. For Vp-p > 2 V, the BER performance shows degradation for both schemes. However, OFDM-PWM is still superior to ACO-OFDM. Since the information is carried in the pulse width, rather than pulse amplitude as in ACO-OFDM, OFDM-PWM displays a higher resiliency to the non-linearity of the LED and clipping, thus offering an improved performance.

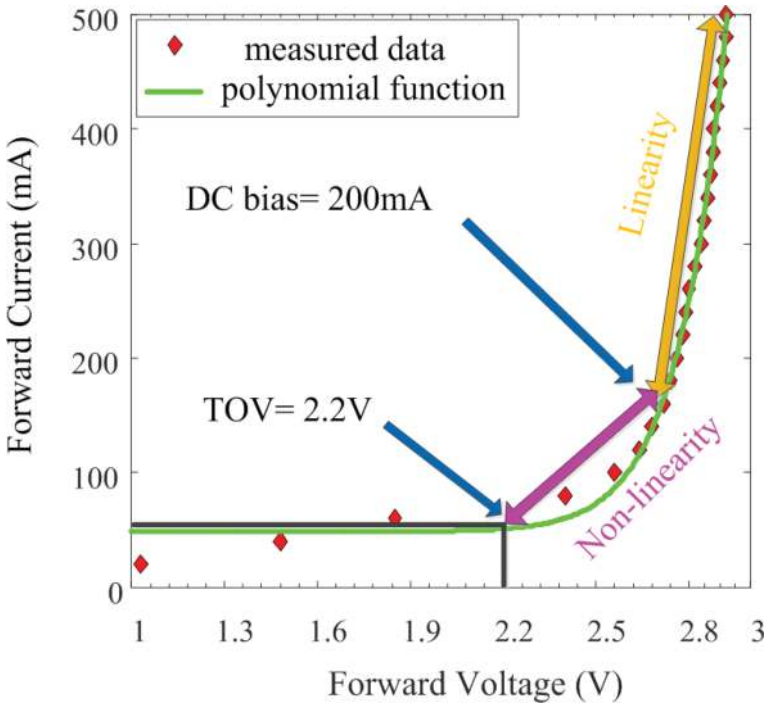

Figure 11. The LED I-V plot using polynomial function (Rebel Star 01, LED). TOV: turn-on voltage.

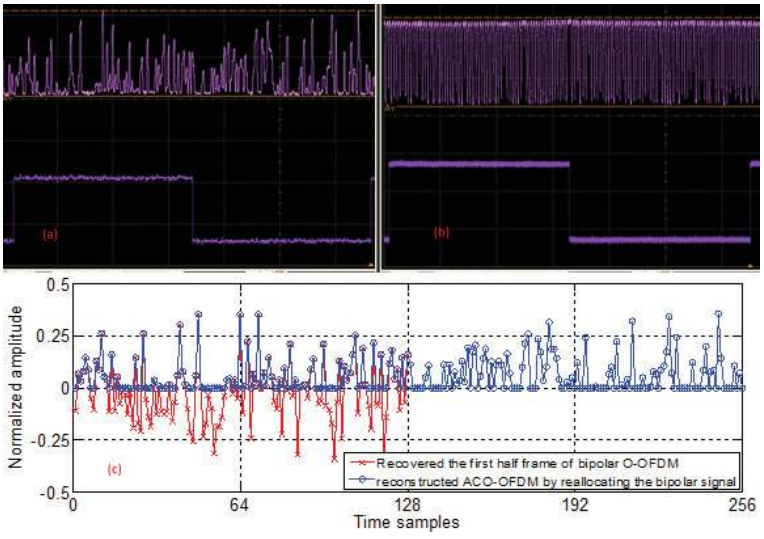

Figure 12. Waveforms of a single frame of 256-subcarrier for: (a) ACO-OFDM, (b) OFDM-PWM with $R = 100$, and (c) the recovered half frame of bipolar signal and the reconstructed ACO-OFDM frame. Note the square wave in (a) and (b) is to show the period of OFDM waveforms.

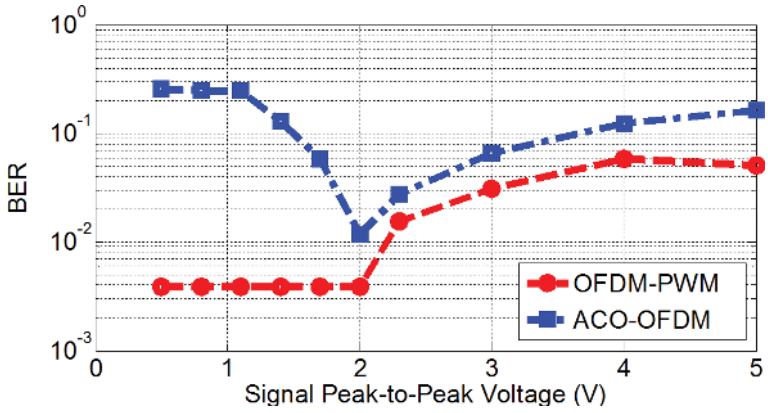

Figure 13. Experimental BER against the peak-to-peak amplitude for 16-QAM OFDM-PWM and ACO-OFDM under the same conditions.

5. Conclusion

In this chapter, we proposed two novel PAPR reduction schemes for O-OFDM-based VLC systems. The first scheme is implemented in the time domain to mitigate the high PAPR experienced in ACO-OFDM, which uses the Gaussian blur method with a Toeplitz matrix-based Gaussian kernel function at the transmitter. We have shown that for 256-subcarrier ACO-OFDM, a ∼6dB improvement in PAPR is achieved in terms of CCDF compared with the original ACO-OFDM. By taking advantage of the special time-domain structure of ACO-OFDM symbols, the OMP algorithm is employed to efficiently recover the original ACO-OFDM signal at the receiver. Simulation results have shown that a ∼6 dB PAPR reduction requires only a ∼2 dB of additional SNR compared to the ideal ACO-OFDM scheme at a BER of 10−4 and with the signal reconstruct error less than 0.1. Then, the second scheme is an improved modulation scheme based on the conversion of an ACO-OFDM signal to PWM. The OFDM-PWM offers significant advantages compared with the traditional ACO-OFDM scheme including lower PAPR, higher luminance, improved BER performance, and enhanced resiliency to the source non-linearity. The simulation and experimental results both show that a significant BER improvement can be achieved with OFDM-PWM compared to ACO-OFDM.

Author details

Tian Zhang[1], Jun Yao[2] and Shuxu Guo[1]*

*Address all correspondence to: guosx@jlu.edu.cn

1 College of Electronic Science and Engineering, Jilin University, Changchun, China

2 Department of Electrical and Computer Engineering, Carnegie Mellon University, Pittsburgh, PA, USA

References

[1] Ghassemlooy Z, Arnon S, Uysal M, Xu Z, Cheng J. Emerging optical wireless communications-advances and challenges. IEEE Journal on Selected Areas in Communications. 2015;**33**(9):17381749/15381761. DOI: 10.1109/JSAC.2015.2458511

[2] Minh HL, O'Brien D, Faulkner G, Zeng L, Lee K, Jung D, Oh Y, Won ET. 100-Mb/s NRZ visible light communications using a postequalized white LED. IEEE Photonics Technology Letters. 2009;**21**(15):10631065/10779028. DOI: 10.1109/LPT.2009.2022413

[3] Dissanayake SD, Armstrong J. Comparison of ACO-OFDM, DCO-OFDM and ADO-OFDM in IM/DD systems. Journal of Lightwave Technology. 2013;**31**(7):10631072/13287715. DOI: 10.1109/JLT.2013.2241731

[4] Kimura H, Asaka K, Nakamura K, Kimura S, Yoshimoto N. Energy efficient IM-DD OFDM-PON using dynamic SNR management and adaptive modulation. Optics Express. 2014;**22**(2):17891795. DOI: https://doi.org/10.1364/OE.22.001789

[5] Jiang T, Wu Y. An overview: Peak-to-average power ratio reduction techniques for OFDM Signals. IEEE Transactions on Broadcasting. 2008;**54**(2):257268/10002861. DOI: 10.1109/TBC.2008.915770

[6] Beril Inan SC, Lee J, Randel S, Neokosmidis I, Koonen AMJ, Walewski JW. Impact of LED nonlinearity on discrete multitone modulation. Journal of Optical Communications and Networking. 2009;**1**(5):439451. DOI: https://doi.org/10.1364/JOCN.1.000439

[7] Mesleh R, Elgala H, Haas H. LED nonlinearity mitigation techniques in optical wireless OFDM communication systems. Journal of Optical Communications and Networking. 2012;**4**(11):865875. DOI: https://doi.org/10.1364/JOCN.4.000865

[8] O'Neill R, Lopes LB. Envelope variations and spectral splatter in clipped multicarrier signals. Toronto: IEEE; 1995; p. 7175. DOI: 10.1109/PIMRC.1995.476406

[9] Kang W, Hranilovic S. Power reduction techniques for multiple-subcarrier modulated diffuse wireless optical channels. IEEE Transactions on Communications. 2008;**56**(2):279288/9836375. DOI: 10.1109/TCOMM.2008.060609

[10] You R, Kahn JM. Average power reduction technique for multiple subcarrier intensity modulated optical signals. IEEE. 2000; pp. 1620–1627, New Orleans, LA, USA. DOI: 10.1109/ICC.2000.853769

[11] Nadal L, Moreolo MS, Fabrega JM, Junyent G. Low complexity bit rate variable transponders based on optical OFDM with PAPR reduction capabilities. Spain: IEEE; 2012; p. 16. DOI: 10.1109/NOC.2012.6249918

[12] Popoola WO, Ghassemlooy Z, Stewart BG. Pilot-assisted PAPR reduction technique for optical OFDM communication systems. Journal of Lightwave Technology. 2014;**32**(7):13741382/14111646. DOI: 10.1109/JLT.2014.2304493

[13] Wasiu O. Popoola; Zabih Ghassemlooy; Brian G. Stewart. Optimizing OFDM based visible light communication for high throughput and reduced PAPR. In: 8–12 June 2015; IEEE; 2015. p. 1322–1326, London, UK. DOI: 10.1109/ICCW.2015.7247361

[14] Zhang T, Ghassemlooy Z, Ma C, Guo S. PAPR reduction scheme for ACO-OFDM based visible light communication systems. Optics Communications. 2017;**383**:7580. DOI: http://dx.doi.org/10.1016/j.optcom.2016.07.073

[15] Flusser J, Farokhi S, Höschl C, Suk T, Zitová B, Pedone M. Recognition of images degraded by Gaussian Blur. IEEE Transactions on Image Processing. 2016;**25**(2):790806/15746081. DOI: 10.1109/TIP.2015.2512108

[16] Zhang T, Ghassemlooy Z, Rajbhandari S, Popoola WO, Guo S. OFDM-PWM scheme for visible light communications. Optics Communications. 2017;**385**:213–218. DOI: http://dx.doi.org/10.1016/j.optcom.2016.10.038

[17] Guerra V, Suarez-Rodriguez C, El-Asmar O, Rabadan J, Perez-Jimenez R. Pulse width modulated optical OFDM. IEEE. 2015; pp. 1333–1337, London, UK. DOI: 10.1109/ICCW.2015.7247363

[18] Armstrong J. OFDM for optical communications. Journal of Lightwave Technology. 2009;**27**(3):189204/10479055. DOI: 10.1109/JLT.2008.2010061

[19] Li F, Wu K, Zou W, Chen J. Optimization of LED's SAHPs to simultaneously enhance SNR uniformity and support dimming control for visible light communication. Optics Communications. 2015;**341**:218–227. DOI: http://dx.doi.org/10.1016/j.optcom.2014.12.025

[20] Rebollo-Neira L, Lowe D. Optimized orthogonal matching pursuit approach. IEEE Signal Processing Letters. 2002;**9**(4):137140/7276019. DOI: 10.1109/LSP.2002.1001652

[21] Han SH, Lee JH. An overview of peak-to-average power ratio reduction techniques for multicarrier transmission. IEEE Wireless Communications. 2005;**12**(2):5665/8389285. DOI: 10.1109/MWC.2005.1421929

[22] Emmanuel J Candes, Michael B Wakin. An introduction to compressive sampling. IEEE Signal Processing Magazine. 2008;**25**(2):2130/9903092. DOI: 10.1109/MSP.2007.914731

[23] Davenport MA, Wakin MB. Analysis of orthogonal matching pursuit using the restricted isometry property. IEEE Transactions on Information Theory. 2010;**56**(9):43954401/11473346. DOI: 10.1109/TIT.2010.2054653

[24] Tony Cai T, Wang L. Orthogonal matching pursuit for sparse signal recovery with noise. IEEE Transactions on Information Theory. 2011;**57**(7):46804688/12068809. DOI: 10.1109/TIT.2011.2146090

[25] Xu W, Wu M, Zhang H, You X, Zhao C. ACO-OFDM-specified recoverable upper clipping with efficient detection for optical wireless communications. IEEE Photonics Journal. 2014;**6**(5):117/14580758. DOI: 10.1109/JPHOT.2014.2352643

[26] Khalid AM, Cossu G, Corsini R, Choudhury P, Ciaramella E. 1-Gb/s transmission over a phosphorescent white LED by using rate-adaptive discrete multitone modulation. IEEE Photonics Journal. 2012;**4**(5):14651473. DOI: 10.1109/JPHOT.2012.2210397

[27] Armstrong J, Schmidt BJC. Comparison of asymmetrically clipped optical OFDM and DC-biased optical OFDM in AWGN. IEEE Communications Letters. 2008;**12**(5):343345/9966259. DOI: 10.1109/LCOMM.2008.080193

[28] Wilson W, Ghassemlooy Z. Pulse time modulation techniques for optical communications: a review. IEE Proceedings J-Optoelectronics. 1993;**140**(6):347357/4587345. DOI: 10.1049/ip-j.1993.0055

[29] Haigh PA, Ghassemlooy Z, Minh HL, Rajbhandari S, Arca F, Tedde SF, Hayden O, Papakonstantinou I. Exploiting equalization techniques for improving data rates in organic optoelectronic devices for visible light communications. Journal of Lightwave Technology. 2012;**30**(19):30813088/13014650. DOI: 10.1109/JLT.2012.2210028